A Numerical Study of Transient Ignition in a Counterflow Nonpremixed Methane-Air Flame using Adaptive Time Integration*

Hong G. Im
Combustion Research Facility, Sandia National Laboratories
Livermore, CA 94551, USA
hgim@sandia.gov

Laxminarayan L. Raja and Robert J. Kee
Engineering Division, Colorado School of Mines
Golden, CO 80401, USA
lraja@mines.edu, rjkee@mines.edu

Linda R. Petzold
University of California
Santa Barbara, CA, 93106 USA
petzold@engineering.ucsb.edu

Keywords: Ignition, Adaptive Time Integration, DAE System

Abstract

This paper presents a computational algorithm to predict highly-transient flame behavior in counterflow situations. The first objective of the paper is to extend the transient counterflow problem to incorporate some gasdynamic compressibility effects, yet retain the desirable similarity structure. By relaxing assumptions in earlier formulations, the computational algorithms can deliver high accuracy even in periods of extremely rapid transients, like combustion ignition. The algorithms are demonstrated on two combustion-ignition problems for methane-air, counterflow, nonpremixed flames. The first concerns the ignition transient in a steady strain field. The second concerns the effects of a high-frequency oscillatory strain field on the ignition process. The results reveal that, when the mean strain rate is near the steady ignition limit, the ignition process is highly sensitive to the details of the strain-rate fluctuations.

*Submitted to *Combustion Science and Technology* (1999).

1. INTRODUCTION

The study of flame structure in counterflow configurations continues to provide important contributions to the understanding of turbulent combustion. This is owing to the well-characterized fluid-mechanical strain field in such flows, allowing efficient computational solution. Thus far, the majority of such investigations are carried out in a steady-state setting. In recent years, however, there has been increasing research interest in the high-frequency transient behaviors associated with ignition and extinction as well as the effects of rapidly varying strain fields on flame structure.

One class of transient combustion problems concerns the autoignition of hydrocarbon fuels, for example in diesel engines or in knocking of spark-ignition engines. Such processes involve complex chemical effects, known as "cool flame" phenomena, as well as fluid dynamic effects including turbulent mixing and dissipation. To assist understanding of flame structure, one-dimensional opposed-flow configuration has been used to study the fluid-dynamic effects, which are often characterized by the strain rate. Such studies (Darabiha and Candel, 1992; Balakrishnan *et al.*, 1995; Kreutz and Law, 1996), however, deal with characterizing ignition limits in a steady context, thereby lacking information of transient ignition history.

Relatively few studies have considered unsteady ignition problems in strained flows. Nieioka (1981) analyzed a thermal-ignition problem with global chemistry, demonstrating that ignition delay is more sensitive to strain-rate variation as the system becomes closer to the steady ignition limit. Analogous behavior was observed in a study considering a hydrogen-air system at high temperatures (Mellado *et al.*, 1999), in which the formal analysis showed that the effect of strain rate is of higher order when the system Damköhler number is sufficiently higher than the critical limit, while more sensitive response was observed near the

ignition limit. It is of interest to examine whether the same behavior can be observed in more complex hydrocarbon systems.

A number of previous investigators have considered counterflow flame structure in time-varying strain fields (Egolfopoulos and Campbell, 1996; Sung and Law, 1997; Im *et al.*, 1999). They have all used a system of equations that is the time-dependent extension of the steady-state counterflow problem. Most of these studies have also used numerical algorithms for time stepping that lack adaptivity in chosing step sizes and therefore incapable of controlling solution error during transient simulations.

Broadly speaking, there are two formulations for the counterflow problems; one involving a single strain-rate parameter that was first discovered by Hiemenz (1911) in the context of a non-reacting stagnation flow past a wall. More recent developments (Dixon-Lewis *et al.*, 1984) have extended the formulation to reacting flows, which have been used to model the counterflow diffusion flame near the stagnation point of a porous cylinder (Tsuji and Yamaoka, 1971). The other formulation, which is adopted in this paper, accounts for a finite separation between the two opposing flow inlets (Kee *et al.*, 1988; Lutz *et al.*, 1996). In the former formulation, the pressure field in the stagnation region is represented as a simple function of an outer potential flow, and therefore depends simply on the strain-rate. In the latter, the pressure field is represented through a pressure-curvature eigenvalue. In both formulations, there is an assumption that the flow is characterized by low Mach numbers and furthermore is *gasdynamically* incompressible, *i.e.* acoustically filtered (see Paolucci, 1982; Majda and Sethian, 1985).

The incompressible formulations work well for relatively mild transients where the time scales of the imposed transients are large in comparison to the acoustic time scales. The calculated pressure field is assumed to respond instantaneously to disturbances in the flow

and details of the acoustic relaxation phenomena are ignored. However, the formulation can be very difficult to solve numerically for very fast transients where the time scales of the imposed flow disturbances are comparable to those for relaxation of the pressure field. Moreover, to accurately capture fast transients like ignition, the computational algorithm must be capable of rigorous error control through automatic and adaptive time-step selection. The discrete form of the equations are represented as differential-algebraic equations (DAE). The assumption of gasdynamic incompressibility manifests itself in the high-index nature of the corresponding discrete equations (DAEs) and numerical difficulty is caused by the inability of the solution algorithms to control local truncation error through automatic time-step selection (Brenan *et al.*, 1996; Ascher and Petzold, 1998).

In this study, we revise the counterflow formulation to reduce the DAE index and thus facilitate high-accuracy numerical solution. The revised formulation was first developed by Raja *et al.* (1998) and successfully applied to the study of catalytic ignition which involve fast transients in wall-bounded stagnation flows. The reformulation has two components – one physical and one algorithmic. By relaxing assumptions of the incompressible-flow formulation to include the acoustic-like pressure adjustments driven by rapid changes in the flow field, the DAE system takes a special form called Hessenberg index-two. Such a system can be further reduced to an index-one system by a simple variable substitution (Ascher and Petzold, 1998). Once in an index-one form, the system is solved accuately and efficiently with the DASPK software, which implements a backward-difference formula (BDF) method with adaptive time-step and order control (Li and Petzold, 1999).

As a physical application of the numerical method, we study transient ignition problems in a methane-air mixing layer. The simulations discussed herein consider ignition in a methane-air mixing layer under two different strain-rate conditions. First, ignition under various

steady strain rate conditions are considered as a baseline study. This is followed by the ignition under oscillatory strain rate with various frequencies in order to understand the effect of flow unsteadiness on ignition behavior. We incorporate detailed C_2 chemistry (Frenklach *et al.*, 1995), thus demonstrating the versatility of the numerical method in a complex chemical system.

In the next two sections, we present the mathematical formulation of the problem. The discussion reviews the compressible stagnation-flow formulation presented in Raja *et al.* (1998) and expands on it within the context of transient counterflow problems.

2. INCOMPRESSIBLE-FLOW FORMULATION: HIGH-INDEX DAE'S

Figure 1 shows a schematic of the system configuration. Two opposing axisymmetric nozzles are separated by a distance of L. The governing equations for the unsteady opposed-flow geometry follows the formulation by Kee *et al.* (1988) derived for the finite-distance opposing nozzles.

We first begin with the low-Mach-number form of the Navier-Stokes equations. In the low-Mach-number limit, the total static pressure, P, can be decomposed into the thermodynamic (p_0) and hydrodynamic (p) components, such that

$$P = p_0 + p, \qquad p/p_0 \ll 1. \tag{1}$$

Furthermore, the flow work and viscous dissipation terms are neglected in the energy equation. We also neglect the possibility of buoyancy-driven recirculations in the flow between the two opposing nozzles and assume that the axial velocity, scaled radial velocity, temperature, and species mass fractions are, respectively, given as a function of time and the axial

coordinate only:

$$u = u(t,x), \quad v/r = V(t,x), \quad T = T(t,x), \quad Y_k = Y_k(t,x). \tag{2}$$

In order to be consistent with the above assumed functional forms, the boundary conditions on u, V, T,and Y_k that are imposed at the nozzle exits need to be independent of radius and therefore fixed constants or functions of time. Substituting these functional forms into the low-Mach-number Navier-Stokes equations, we obtain the following reduced equations

Mass continuity:

$$\frac{\partial \rho}{\partial t} + \frac{\partial}{\partial x}(\rho u) + 2\rho V = 0, \tag{3}$$

Radial momentum:

$$\rho \frac{\partial V}{\partial t} + \rho u \frac{\partial V}{\partial x} + \rho V^2 - \frac{\partial}{\partial x}\left(\mu \frac{\partial V}{\partial x}\right) + \Lambda = 0, \tag{4}$$

Energy conservation:

$$\rho c_p \frac{\partial T}{\partial t} + \rho c_p u \frac{\partial T}{\partial x} - \frac{\partial}{\partial x}\left(\lambda \frac{\partial T}{\partial x}\right) - \frac{\partial p_0}{\partial t} + \rho(\sum_k c_p Y_k V_k)\frac{\partial T}{\partial x} + \sum_k h_k W_k \omega_k = 0, \tag{5}$$

Species conservation:

$$\rho \frac{\partial Y_k}{\partial t} + \rho u \frac{\partial Y_k}{\partial x} + \frac{\partial}{\partial x}(\rho Y_k V_k) - W_k \omega_k = 0, \quad k = 1, \cdots, K, \tag{6}$$

where the radial pressure-curvature eigenvalue,

$$\Lambda(t) \equiv \frac{1}{r}\frac{\partial p}{\partial r}, \tag{7}$$

is a time-dependent variable that is determined as part of the solution. In these equations, Y_k is the mass fraction of species k, c_p is the specific heat of the mixture, λ is the thermal conductivity of the mixture, h_k is the enthalpy of species k, and W_k is the molecular weight of species k.

Note that the above equations are completely independent of r and hence the original assumption on the functional form of the dependent variables, Eq. (2), is valid. The above equations are therefore in a *similarity* form. Consistent with the low-Mach-number approximation, the fluid density is determined from the approximate form of the equation of state:

$$\rho = p_0 \overline{W} / RT, \tag{8}$$

where $\overline{W}$ is the mixture-averaged molecular weight, and the pressure is approximated by the uniform thermodynamic pressure $p_0(t)$. The density therefore depends only on the the axial coordinate and time, *i.e.* $\rho = \rho(x,t)$, which in turn facilitates derivation of the above similarity equations. It is also noted that the axial momentum equation is left out from the above governing equations. In fact, the axial momentum equation can be included to determine the axial dependence of the pressure. However, the axial momentum equation is decoupled form the rest of the system since it does not affect the rest of the solution field.

As a numerical convenience to maintain the banded structure of the iteration matrix, a trivial equation

$$\frac{\partial \Lambda}{\partial x} = 0 \tag{9}$$

is added, simply requiring that Λ is independent of x.

Other constitutive relations include the diffusion velocity, V_k, given by either the multicomponent formulation

$$V_k = \frac{1}{X_k \overline{W}} \sum_{j=1}^{K} W_j D_{kj} \frac{dX_j}{dx} - \frac{D_k^T}{\rho Y_k} \frac{1}{T} \frac{dT}{dx}, \tag{10}$$

or the mixture-averaged formulation

$$V_k = -\frac{1}{X_k} D_{km} \frac{dX_k}{dx} - \frac{D_k^T}{\rho Y_k} \frac{1}{T} \frac{dT}{dx} \quad \text{where} \quad D_{km} = \frac{1 - Y_k}{\sum_{j \neq k}^{K} X_j / \mathcal{D}_{jk}}, \tag{11}$$

where D_{kj}, D_{km}, $\mathcal{D}_{jk}$ and D_k^T are the multicomponent, binary and mixture-averaged and thermal-diffusion coefficients, respectively, and X_k is the mole fraction of species k.

The above system of equations is subject to boundary conditions

$$\begin{aligned} x = 0: \quad & u = u_F(t), \quad V = V_F(t), \quad T = T_F(t), \quad Y_k = (Y_k)_F(t), \\ x = L: \quad & u = u_O(t), \quad V = V_O(t), \quad T = T_O(t), \quad Y_k = (Y_k)_O(t), \end{aligned} \tag{12}$$

where subscripts F and O denote the fuel and oxidizer streams, respectively. In the present formulation of finite nozzle spacing, both axial and radial velocity can be independently prescribed at the boundary, although $V = 0$ is the most common choice for practical cases. Note that the mass continuity equation is first-order and hence takes only one of the axial velocity boundary conditions (say $u_F(t)$). The other axial velocity boundary condition (say $u_O(t)$) is associated with the trivial equation, Eq. (9), which otherwise has no explicit boundary condition. Also, in specifying boundary conditions on the species mass fractions care must be exercised to ensure that $\sum Y_k = 1$.

From a mathematical standpoint, Eqs. (3) - (6) and (9) after spatial discretization are viewed as a system of differential-algebraic equations with a dependent-variable vector $[u_j, V_j, T_j, (Y_k)_j, \Lambda]^T$, where the subscript j denotes grid points that range from 1 to J. Note that, in the analysis of the DAE's, all discrete Λ_j's can be expressed in terms of one Λ without loss of generality. In this case, u_j and Λ constitute the algebraic variables, *i.e.* variables that are not expressed in terms of their time derivatives in the governing equations. The vector of dependent variables is thus divided into two groups as

$$\begin{aligned} \mathbf{x} &= [V_1, T_1, (Y_k)_1, \cdots, V_J, T_J, (Y_k)_J]^T \\ \mathbf{z} &= [u_1, \cdots, u_J, \Lambda]^T \end{aligned} \tag{13}$$

where $\mathbf{x}$ is the vector of all differential variables and $\mathbf{z}$ is the vector of all algebraic variables. Note that the boundary condition on V, T and Y_k specified in Eq. (12) can be represented in terms of their time derivatives and hence these boundary variables can be considered

as differential variables. For example, specifying T_J = constant is equivalent to specifying $dT_J/dt = 0$ with a proper initial condition, *i.e.* $T_J(t = 0)$ = constant. The DAE system for the discretized counterflow equations can then be written as:

$$\begin{aligned} \frac{d\mathbf{x}}{dt} &= \mathbf{f}(\mathbf{x}, \mathbf{z}) \\ 0 &= \mathbf{g}(\mathbf{x}, \mathbf{z}), \end{aligned} \tag{14}$$

where $\mathbf{f}$ represents the right hand sides of all the differential equations (*i.e.* equations for the radial momentum, energy conservation, and species conservation at the interior nodes and equivalent differential equations for boundaries conditions on V, T and Y_k) and $\mathbf{g}$ represents the algebraic equations (*i.e.* the mass continuity at all interior and boundary nodes).

For the DAE system to be at least index-2, the product of the Jacobian matrices $\mathbf{g_x f_z}$ must be nonsingular (Brenan *et al.*, 1996; Ascher and Petzold, 1998). This is not the case for the above DAE system. The algebraic equation corresponding to the discretized continuity at the boundaries do not have any term belonging to $\mathbf{x}$ and therefore at least one row of the Jacobian matrix $\mathbf{g_x}$ is zero. Consequently, the requisite product of the matrices is singular and the DAE system is of index greater than 2 – the cause of numerical difficulties in fast-transient problems.

3. COMPRESSIBLE-FLOW FORMULATION WITH INDEX REDUCTION

The index of the DAE system can be reduced by reformulating the problem to include the appropriate physical phenomena that are valid in the regime of interest. Under fast transient conditions, a local flow disturbance (as occuring in the ignition event) is first communicated to the surrounding flow through acoustic pressure waves. On longer time scales, information is communicated through convective and diffusive transport. The incompressible formulation (acoustically-filtered equations) assumes that the pressure waves are infinitely fast,

communicating information instantly throughout the flow, which is the root cause of the high-index behavior. To reduce the index, some compliance must be introduced into the system, allowing a slower, and more physical, response to a disturbance. That is, the axial pressure distribution must be coupled back into the dynamics of the flow, in addition to the radial pressure effect represented by the eigenvalue, Λ.

Once recognized, this is easily done by reintroducing pressure as a dependent variable and coupling back the axial momentum equation in the set of governing equations. The excess pressure,

$$p = P - p_0, \tag{15}$$

is now included in the set of dependent variables to obtain the following set of counterflow similarity equations:

Mass continuity:

$$\frac{\rho}{P}\frac{\partial p}{\partial t} - \frac{\rho}{T}\frac{\partial T}{\partial t} - \rho\overline{W}\sum_k \frac{1}{W_k}\frac{\partial Y_k}{\partial t} + \frac{\partial}{\partial x}(\rho u) + 2\rho V = 0, \tag{16}$$

Axial momentum:

$$\rho\frac{\partial u}{\partial t} + \rho u\frac{\partial u}{\partial x} + \frac{\partial p}{\partial x} - 2\mu\frac{\partial V}{\partial x} - \frac{4}{3}\frac{\partial}{\partial x}\left(\mu\frac{\partial u}{\partial x}\right) + \frac{4}{3}\frac{\partial}{\partial x}(\mu V) = 0, \tag{17}$$

Radial momentum:

$$\rho\frac{\partial V}{\partial t} + \rho u\frac{\partial V}{\partial x} + \rho V^2 - \frac{\partial}{\partial x}\left(\mu\frac{\partial V}{\partial x}\right) + \Lambda = 0, \tag{18}$$

Energy conservation:

$$\rho c_p\frac{\partial T}{\partial t} + \rho c_p u\frac{\partial T}{\partial x} - \frac{\partial}{\partial x}\left(\lambda\frac{\partial T}{\partial x}\right) - \frac{\partial P}{\partial t} + \rho(\sum_k c_p Y_k V_k)\frac{\partial T}{\partial x} + \sum_k h_k W_k\omega_k = 0, \tag{19}$$

Species conservation:

$$\rho\frac{\partial Y_k}{\partial t} + \rho u\frac{\partial Y_k}{\partial x} + \frac{\partial}{\partial x}(\rho Y_k V_k) - W_k\omega_k = 0, \quad k = 1, \cdots, K. \tag{20}$$

The equation of state is also modified as

$$\rho = (p + p_0)\,\overline{W}/RT, \tag{21}$$

where the pressure term now includes the excess pressure p. The mass continuity equation now includes the time derivative of p that is derived by differentiation of the new equation of state. It is also noted that the magnitude of the viscous terms in the axial momentum equation is very small for problems of interest and can be neglected without loss of solution accuracy.

In addition to the boundary conditions, Eq. (12), a new boundary condition must be specified for pressure. For flow situations without any imposed nozzle exit velocity perturbations, it is convenient to specify $p = 0$ at one of the boundaries, *e.g.* at $x = L$. For flows with exit velocity perturbations, we adopt the Bernoulli's equation

$$p_J + \frac{1}{2}\rho_J u_J^2 = \text{constant}. \tag{22}$$

For the compressible equations, the $u = u_O(t)$ boundary condition is associated with the axial momentum equation and the pressure boundary condition is associated with the trivial equation for Λ, Eq. (9). See Figure 2 for details on specification of the boundary conditions.

The set of dependent variables in the discretized compressible equation can be divided into two groups as follows

$$\begin{aligned} \mathbf{x} &= [p_1, u_1, V_2, T_2, (Y_k)_2, \cdots, p_J, u_J, V_J, T_J, (Y_k)_J]^T \\ \mathbf{z} &= [\Lambda]. \end{aligned} \tag{23}$$

The DAE system for the compressible equation can now be expressed as

$$\begin{aligned} \frac{d\mathbf{x}}{dt} &= \mathbf{f}(\mathbf{x}, \mathbf{z}) \\ 0 &= \mathbf{g}(\mathbf{x}). \end{aligned} \tag{24}$$

The vector $\mathbf{f}$ represents the right hand sides of all the differential equations for axial momentum, radial momentum, energy conservation, and species conservation at the interior nodes and equivalent differential equations for boundaries conditions on u, V, T and Y_k. The vector $\mathbf{f}$ also includes the differential equations for the mass continuity equations at all interior nodes and the bottom boundary $x = 0$. The vector $\mathbf{g}$ represents the single algebraic equation, Eq. (22), which is used as the equation for Λ.

Through an analysis of the DAE system, Eq. (24), it can be shown that the product of Jacobian matrices $\mathbf{g_x f_z}$ is nonsingular and hence the equations are in a special Hessenberg index-2 form (Brenan *et al.*, 1996; Ascher and Petzold, 1998). Theory also suggests that, once in this form, the DAE index can be further reduced to index-1 using the simple substitution

$$\frac{d\phi}{dt} = \Lambda(t). \tag{25}$$

The variable ϕ replaces Λ as the dependent variable and any arbitrary initial condition can be specified for ϕ, since only $d\phi/dt$ appears in the system of equations (Ascher and Petzold, 1998). The discretized index-1 compressible counterflow equations are numerically stable in fast-transient regimes and can be solved efficiently using adaptive time-stepping algorithms capable of solution error control.

4. NUMERICAL METHODS

The DAE system, Eqs. (16) - (20), can be solved numerically using DASPK. Since DASPK requires that the initial condition must satisfy all the equations in the DAE system, a fully converged steady solution field is used as the initial condition. Due to the modified grid structure as described in the following, a modified version of OPPDIF is used to obtain the initial condition.

To fit the modified formulation, a staggered grid system is used as shown in Figure 2. The grid stencil and boundary conditions for individual dependent variables are shown in separate columns. All dependent variables are represented at the control-volume center nodes, except the axial velocity which is represented at the control-volume faces. The grid indices are shown on the left and the face indices on the right. The right-facing protuberance on the stencils indicates where the time derivative is evaluated. For the pressure-eigenvalue equation there is no time derivative, as indicated by an unfilled protuberance.

Spatial discretization uses finite-volume differencing for the non-uniform grid system. For the species, energy, and radial momentum equations, a second-order central differencing is used for diffusive terms, and either first-order upwind or second-order central differencing is used for the convective terms. The continuity equation is spatially first order, using a central difference formulation with u at the cell surfaces. Although the axial momentum equation is second order in velocity through the viscous term, the important convective term is first order. The equation is therefore treated as a first-order equation by either neglecting the viscous terms entirely or by interpreting them as source terms.

Because the central differencing on the continuity equation is only neutrally stable, an artificial damping term is introduced to maintain numerical stability. A first-order damping term of the form $\sigma(\Delta x)(\partial^2 p/\partial x^2)$ is added in the continuity equation, where a sufficiently small value for σ is used to ensure that the solution is not affected. From our experience, $\sigma \approx 10^{-3}$ appears to be acceptable without noticeably affecting the final solution.

The unsteady calculation requires a fully converged steady solution as an initial condition. To accommodate the transient response of the reaction zone, an *a priori* grid refinement is needed, as described in the following (Lutz *et al.*, 1996).

First, a grid redistribution by a weighting function is made. Temperature is typically used

as the gauge variable and the grid redistribution uses a transformation from the physical coordinate x to a new coordinate η,

$$\frac{dx}{d\eta} W(x,T) = C \tag{26}$$

with the weighting function

$$W(x,T) = 1 + b_1 \left| \frac{dT}{dx} \right| + b_2 \left| \frac{d^2T}{dx^2} \right|. \tag{27}$$

The constant C is defined by the integration over the entire domain:

$$C = \frac{1}{N-1} \int_0^L W(x,T) dx, \tag{28}$$

where N is the total number of grid points. Integrating over a portion of the domain gives an expression for the locations in the η-coordinate space:

$$\eta = 1 + \frac{1}{C} \int_0^x W(x,T) dx. \tag{29}$$

The new grid locations, x, are obtained by interpolation between the computed values of η defined using the old mesh, onto a uniform mesh in the η-space. Since $d\eta$ is constant on this uniform mesh, the solution to Eq. (26) states that $W(x,T) \cdot x$ is constant, so that the new values of x are concentrated where the weighting function is large. The parameters, b_1, b_2 and C are adjusted to produce a desired grid system.

5. RESULTS AND DISCUSSION

Ignition under Constant Strain Rate

We first consider the ignition of a pure methane stream flowing against a hot air stream. The nozzle separation is fixed at $L = 1$ cm and the nominal pressure is $p = 1$ atm. The fuel-side inlet temperature is held at 300K and the hot-air inlet temperature is at 1400K, which is the

ignition heat source. The simulation begins by determining the steady-state non-reacting flow field. For this initial flow field, the chemical reaction rates are simply turned off in the simulation. Then, to initiate the ignition problem, the chemical reaction rates are suddenly turned on. The problem is contrived in the sense that there is no equivalent experiment that can be done. Nevertheless, the results reveal some limiting-case behavior for an ignition transient.

In this paper, the characteristic flow time is represented by the scalar dissipation rate,

$$\chi_{\rm st} = 2\lambda(\partial\xi/\partial x)^2_{\rm st} \tag{30}$$

where λ is the thermal conductivity, ξ is the mixture-fraction variable based on the formula by Bilger (1988), and subscript "st" denotes the stoichiometric condition. It could be argued that the scalar dissipation rate evaluated at the actual ignition location might be a more appropriate measure of the flow time for ignition problems. However, in practice it is difficult to establish unambiguously the "point" of ignition since such a point moves during the course of the ignition. Moreover, it has been shown that $\chi_{\rm st}$ better represents the flow time scale than the strain rate measured far upstream for highly transient flow conditions (Im *et al.*, 1999).

Figure 3 shows the maximum steady-state H-atom mole fraction within the flow as a function the characteristic flow time, represented as the stoichiometric scalar dissipation rate. There are two solution branches – the flame branch where intense diffusion flame is established and the frozen branch where the chemical reaction is suppressed due to insufficient flow residence time. The asymptotically vertical shape of the frozen branch indicates an ignition turning point. Under the conditions used in the present study, this steady ignition limit is found to be at $\chi_{\rm st} = 17.2$ sec^{-1}, which occurs at $u_F = u_O = 2.17$ m/s.

Based on the steady response shown in Figure 3, we first investigate the transient ignition response under various values of constant pre-ignition scalar dissipation rates. For a system to be ignitable, χ_{st} must be lower than the steady ignition limit of 17.2 s_{-1}. The procedure is as follows. Initially a steady, non-reacting flow field is established by artificially supressing all the reaction rates. Then, to initiate the ignition event, the reaction rates are restored. A series of such simulations are done for different pre-ignition scalar dissipation rates.

Figure 4 illustrates the results of an ignition transient for $\chi_{st} = 7.06\ s^{-1}$. Spatial profiles of temperature and H-atom mole fraction are shown for several times during the ignition. For these conditions, the ignition develops over a time span of around 0.4 milliseconds (curves B through E). The ignition kernel develops and propagates into the location at which the steady diffusion flame is established. To further illustrate the ignition transient, the temporal evolution of the spatial maximum values for temperature and a two intermediate species (H and HCO) are shown in Figure 5. Again, the transient takes a few tenths of a millisecond to proceed from a non-burning situation to a steady flame structure. The H and the HCO have fundamentally different behaviors during the transient, with the HCO having a sharp, short-lived peak.

From a numerical or algorithmic point of view, it is clear the differential-equation solver must be able to accommodate periods of very rapid transients during the ignition, yet relatively slow response before and after the ignition itself. Such behavior is characteristic of stiff problems. To be efficient, the solver must choose large time steps during periods or slow change but quickly adjust to smaller timesteps as the solution changes rapidly. The time-step selection must be governed to control the local truncation error in the solution and thus return accurate solutions throughout the course of the ignition. The DASPK software is specifically designed to meet these challenges.

It is convenient to characterize the ignition in terms of an ignition-delay time. In this study, the ignition delay is defined as the time at which the rate of temperature rise becomes maximum. Figure 6 shows the variation of the ignition delay for a range of scalar dissipation rates. Clearly, as the characteristic flow time is reduced to approach the steady ignition limit, the ignition delay becomes increasingly sensitive to the variations in the scalar dissipation rate.

Therefore, the transient ignition exhibits behaviors that cannot be easily described in the steady-state ignition concepts, like the turning point illustrated in Figure 3. For example, many ignition models in turbulent reacting flows are based on the notion that ignition occurs instantaneously when the local scalar dissipation rate at the ignition kernel falls below the steady ignition limit. However, Figure 6 suggests that this assumption may lead to an incorrect prediction, since ignition delay is a strong function of the flow strain especially near the onset of ignition. It is expected that both the absolute value of strain rate and the characteristic time scale of the flow unsteadiness may significantly affect the ignition response. This issue is investigated further in the next section.

Ignition under Oscillatory Strain Rates

To study the effect of time-varying strain rates, which may better represent the action of turbulent eddies, we now investigate the ignition behavior when the system is subjected to an oscillatory flow field of the form

$$u_F(t) = u_O(t) = u_0\{1 + A[1 - \cos(2\pi f t)]\} \tag{31}$$

such that the velocity varies sinusoidally from u_0 to $u_0(1 + 2A)$ at a frequency of f Hz. In these simulations, both inlet velocities oscillate in phase and with the same function. Based on the results with constant scalar dissipation rates shown in Figure 6, we choose two cases

of the initial non-reacting solution field: (A) $u_0 = 1.0$ m/sec, $A = 0.15$, and (B) $u_0 = 2$ m/sec, $A = 0.075$, such that the former is far from the steady ignition limit and the latter near the ignition limit. The respective range of velocity oscillation is drawn as the arrows bounded by dotted lines in Figure 6. Each case was run for several frequencies ranging from 10 to 1000 Hz.

Figures 7 and 8 show the temporal evolution of the maximum temperature and scalar dissipation rate at the stoichiometric point, respectively, for case A. The results in Figure 8, showing the scalar dissipation rate, clearly demonstrate the need for adaptive time steps in the solution algorithm. Just at the ignition time, the solutions are characterized by very fast transients ane periods of very high curvature (sharp peaks). A less sophisticated algorithm would have very great difficulty following these features, and possibly deliver incorrect or misleading solutions.

The temperature response in Figure 7 shows a monotonic increase in the ignition delay as the oscillation frequency increases, although it appears to level off to an asymptotic limit for higher frequencies. Figure 8 shows the effect of transient strain rate more clearly. In the low-frequency case ($f = 10$ Hz), ignition occurs even before any substantial increase in the strain rate is achieved. As the frequency increases, however, the strain-rate oscillation goes through a number of cycles before the ignition point, hence resulting in a net strain rate higher than that for the low-frequency case. Considering the steady-state results shown in Figure 6 that the ignition delay increases monotonically with the strain rate, it is expected that the higher frequency case would produce longer ignition delays, since the system is subjected to higher net strain rates. Nevertheless, for situations where the oscillatory strain rates are far from the steady ignition limit, as illustrated in Figure 7, the strain-rate fluctuation has a relatively small net effect on the ignition delay, notwithstanding the very different scalar

dissipation rate histories as illustrated in Figure 8. This behavior can be understood from the steady response shown in Figure 6. In the low strain-rate range, the characteristic flow residence time is sufficiently large such that the chemical reactions are little affected by the convective/diffusive transport variation.

When the fluctuating strain rate is near the steady ignition limit, however, the ignition becomes quite sensitive to flow-field fluctuations. Figures 9 and 10 show the temporal evolution of the maximum temperature and scalar dissipation rate, respectively, for case B. At $f = 10$ Hz, the ignition occurs before any significant effect of the strain rate oscillation, hence the ignition delay is close to that for the steady case at $u_0 = 2.0$ m/sec at approximately 15 milliseconds. At $f = 100$ Hz, the scalar dissipation rate oscillates a number of cycles before the ignition, thereby influencing the history of scalar dissipation rate throughout the course of the ignition event. In this case, the maximum temperature exhibits a gradual increase throughout a number of cycles and eventually ignition occurs, albeit at much later time (81 milliseconds). At frequencies $f = 200$ Hz and higher, however, the peak temperature reaches a limit cycle at a mean value about 1410 K and ignition is not achieved.

Note that the dramatic difference between the situation at $f = 100$ Hz and 200 Hz is not due to an increase in the mean scalar dissipation rate for higher frequencies; for all frequencies between 100 and 300 Hz, the mean scalar dissipation rate is approximately 7.0 sec^{-1}, which is slightly lower than the steady ignition limit. Therefore, in terms of the mean values, all higher frequency cases ($f = 200$ Hz and higher) may be expected to ignite. The principal distinction between the ignited and unignited cases is the *duration* for which the scalar dissipation rate is less than the steady ignition limit. This implies that, for $f = 100$ Hz, the duration is long enough to build up the radical pool throughout a number of oscillations, while it is not so for higher frequencies. This result is consistent with an earlier study by

Sung and Law (1997), in which they found that ignition occurs when such a duration (called the "excursion time" in their paper) is longer than the characteristic runaway time. Our study differs from that of Sung and Law's in that our initial condition is in an ignitable state ($\chi_{st} < 17.2$ sec^{-1}). As a result, it is difficult to define a characteristic runaway time.

The results shown throughout Figures 7 to 10 may suggest the following implications in application to ignition in turbulent flows. When the mean effective strain rate induced by turbulence is sufficiently lower than the steady ignition limit, the ignition delay is little affected by turbulence. This may explain some earlier observations in direct numerical simulations (Mastorakos *et al.*, 1997; Im *et al.*, 1998), where the turbulence intensity was limited to weak to moderate range. To have a significant effect on ignition delay, the turbulence intensity must be sufficiently large so that the mean value is near the steady ignition limit. Under these circumstances, it is expected that ignition delay is substantially modified by the strain-rate fluctuation, both in amplitude as well as frequency. In an extreme case, it is conceivable to have non-igniting situation even if the mean strain rate is less than the steady ignition limit, demonstrating the importance of unsteady flow effects.

6. CONCLUSIONS

Numerical simulation of one-dimensional unsteady opposed-flow is accomplished using an algorithm and software that is designed for differential-algebraic systems. The commonly-used, acoustically-filtered, counterflow formulation leads to numerical difficulties during periods of very rapid transients in the solution, such as during an ignition event. In this paper, we reformulate the counterflow problem to incorporate some weakly compressible effects, yet retain the desirable one-dimensional similarity structure. As a result, the index of the DAE system is reduced to one, which alleviates numerical difficulties associated with a high-index

system. The numerical method is implemented using the DASPK software. The CHEMKIN software (Kee *et al.*, 1991) provides the means for dealing with complex chemical mechanisms and transport properties.

The paper illustrates the numerical algorithms by simulating two ignition problems, both in a counterflow configuration forming a nonpremixed methane-air flame. In the first case, ignition is simulated in an initially steady flow field. In the second case, the flow velocity for both inlet streams is forced to follow an in-phase oscillation of varying amplitudes and frequencies.

The results for constant strain rate show that the functional dependence of the ignition delay on the strain rate becomes more sensitive as the flow condition approaches the steady ignition limit. The calculations for ignition under oscillatory strain rates further reveal that, while the ignition delay is insensitive to the strain rate fluctuation when it is far from the steady ignition limit, the effect can be greatly amplified as mean strain rate approaches the limit. In some extreme cases, it is shown that high-frequency oscillation can lead to a non-igniting system whose mean strain rate is less than the steady ignition limit. Further study is needed to understand the effect of such parameters in a more realistic multi-dimensional turbulent flow field at elevated turbulence intensities.

Acknowledgment

At Sandia this work has been supported by the US Department of Energy, Office of Basic Energy Sciences, Chemical Sciences Division. At the Colorado School of Mines, the work is supported by NASA, through the CCACS program. The authors would like to thank Dr. A. E. Lutz of Sandia National Laboratories for his assistance in the development of the numerical method.

References

Ascher, U. M. and Petzold, L. R. (1998). *Computer Methods for Ordinary Differential Equations and Differential-Algebraic Equations*, SIAM, Philadelphia, PA.

Bilger, R. W. (1988). The Structure of Turbulent Nonpremixed Flames. *Twenty-Second Symposium (International) on Combustion*, The Combustion Institute, Pittsburgh, PA, pp. 475-488.

Balakrishnan G., Smooke, M. D. and Williams, F. A. (1995). A Numerical Investigation of Extinction and Ignition Limits in Laminar Nonpremixed Counterflowing Hydrogen-Air Streams for Both Elementary and Reduced Chemistry. *Combustion and Flame* **102**, 329-340.

Brenan, K. E., Campbell, S. L. and Petzold, L. R. (1996). *Numerical Solution of Initial-Value Problems in Differential Algebraic Equations*, 2nd ed., SIAM, Philadelphia, PA.

Darabiha, N. and Candel, S. (1992). The Influence of the Temperature on Extinction and Ignition Limits of Strained Hydrogen-Air Diffusion Flames. *Combust. Sci. Tech.* **86**, 67-85.

Dixon-Lewis, G., David, T., Gaskell, P. H., Fukutani, S., Jinno, H., Miller, J. A., Kee, R. J., Smooke, M. D., Peters, N., Effelsberg, E., Warnatz, J. and Behrendt, F. (1984). Calculation of the Structure and Extinction Limit of a Methane-Air Counterflow Diffusion Flame in the Forward Stagnation Region of a Porous Cylinder. *Twentieth Symposium (International) on Combustion*, The Combustion Institute, Pittsburgh, PA, pp. 1893-1904.

Egolfopoulos, F. N. and Campbell, C. S. (1996). Unsteady Counterflowing Strained Diffusion Flames: Diffusion-Limited Frequency Response. *J. Fluid Mech.* **318**, 1-29.

Frenklach, M., Wang, H., Goldenberg, M., Smith, G. P., Golden, D. M., Bowman, C. T., Hanson, R. K., Gardiner, W. C. and Lissianski, V. (1995). GRI-Mech—An Optimized Detailed Chemical Reaction Mechanism for Methane Combustion. *GRI Report* No. GRI-95/0058.

Hiemenz, K. (1911). Die Grenzschicht an einem in der gleichformigen Flussigkeitsstrom eingetauchten geraden Kreiszylinder. *Dingler's Polytech. J.* **326**, 321.

Im, H. G., Chen, J. H. and Chen, J.-Y. (1999). Chemical Response of Methane/Air Diffusion Flames to Unsteady Strain Rate. *Combustion and Flame* **118**, pp. 204-212.

Im, H. G., Chen, J. H. and Law, C. K. (1998). Ignition of Hydrogen-Air Mixing Layer in Turbulent Flows. *Twenty-Seventh Symposium (International) on Combustion*, The Combustion Institute, Pittsburgh, PA, pp. 1047-1056.

Mastorakos, E., Baritaud, T. A. and Poinsot, T. J. (1997). Numerical Simulations of Autoignition in Turbulent Mixing Flows. *Combustion and Flame* **109**, pp. 198-223.

Kee, R. J., Miller, J. A., Evans, G. H. and Dixon-Lewis, G. (1988). A Computational Model of the Structure and Extinction of Strained, Opposed Flow, Premixed Methane-Air Flames. *Twenty-Second Symposium (International) on Combustion*, The Combustion Institute, Pittsburgh, PA, pp. 1479-1494.

Kee, R. J., Rupley, F. M. and Miller, J. A. (1991). Chemkin-II: A Fortran Chemical Kinetics Package for the Analysis of Gas-Phase Chemical Kinetics. *Sandia Report* SAND89-8009B.

Kreutz, T. G. and Law, C. K. (1996). Ignition in Nonpremixed Counterflowing Hydrogen versus Heated Air: Computational Study with Detailed Chemistry. *Combustion and Flame* **104**, 157-175.

Li, S. and Petzold, L. R. (1999). Design of New DASPK for Sensitivity Analysis. *Technical Report of Computer Science Department* (TRCS99-23), University of California, Santa Barbara.

Lutz, A. E., Kee, R. J., Grcar, J. F. and Rupley, F. M. (1996). OPPDIF: A Fortran Program for Computing Opposed-flow Diffusion Flames. *Sandia Report* SAND96-8243.

Mellado, D. J., Sánchez, A. L., Kim, J. S. and Im, H. G. (1999). High-Temperature Radical Growth in the Hydrogen-Oxygen Counterflow Mixing Layer. *17th International Colloquium on the Dynamics of Explosions and Reactive Systems*, Heidelberg, Germany, July 25-30.

Niioka, T. (1981). Ignition Time in the Stretched-Flow Field. *Eighteenth Symposium (International) on Combustion*, The Combustion Institute, PA, pp. 1807-1813.

Paolucci, S. (1982). On the Filtering of Sound from the Navier-Stokes Equations. *Sandia Report* SAND82-88257.

Raja, L. L., Kee, R. J. and Petzold, L. R. (1998). Simulation of the Transient, Compressible, Gas-Dynamic, Behavior of Catalytic-Combustion Ignition in Stagnation Flows. *Twenty-Seventh Symposium (International) on Combustion*, The Combustion Institute, Pittsburgh, PA, pp. 2249-2257.

Sung, C. J. and Law, C. K. (1997). Ignition of Oscillatory Counterflowing Nonpremixed Hydrogen against Heated Air. *Combust. Sci. Tech.* **129**, 347-370.

Tsuji, H. and Yamaoka, I. (1971). *Thirteenth Symposium (International) on Combustion*, The Combustion Institute, Pittsburgh, PA, pp. 723-731.

List of Figures

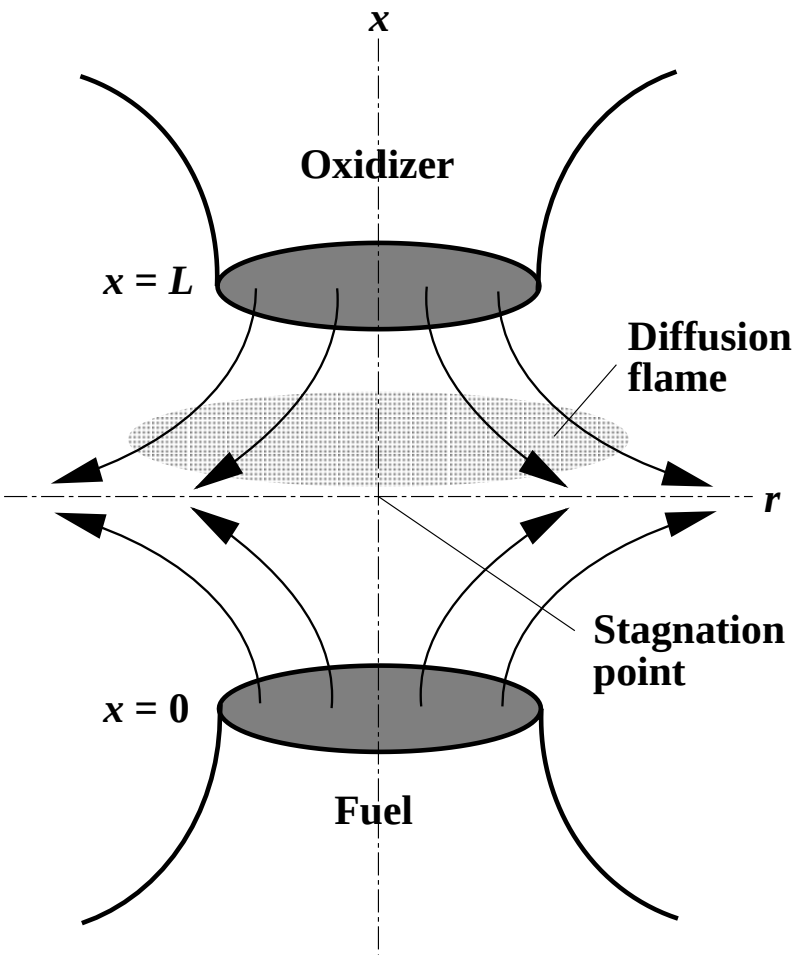

Figure 1: Schematic of the system configuration.

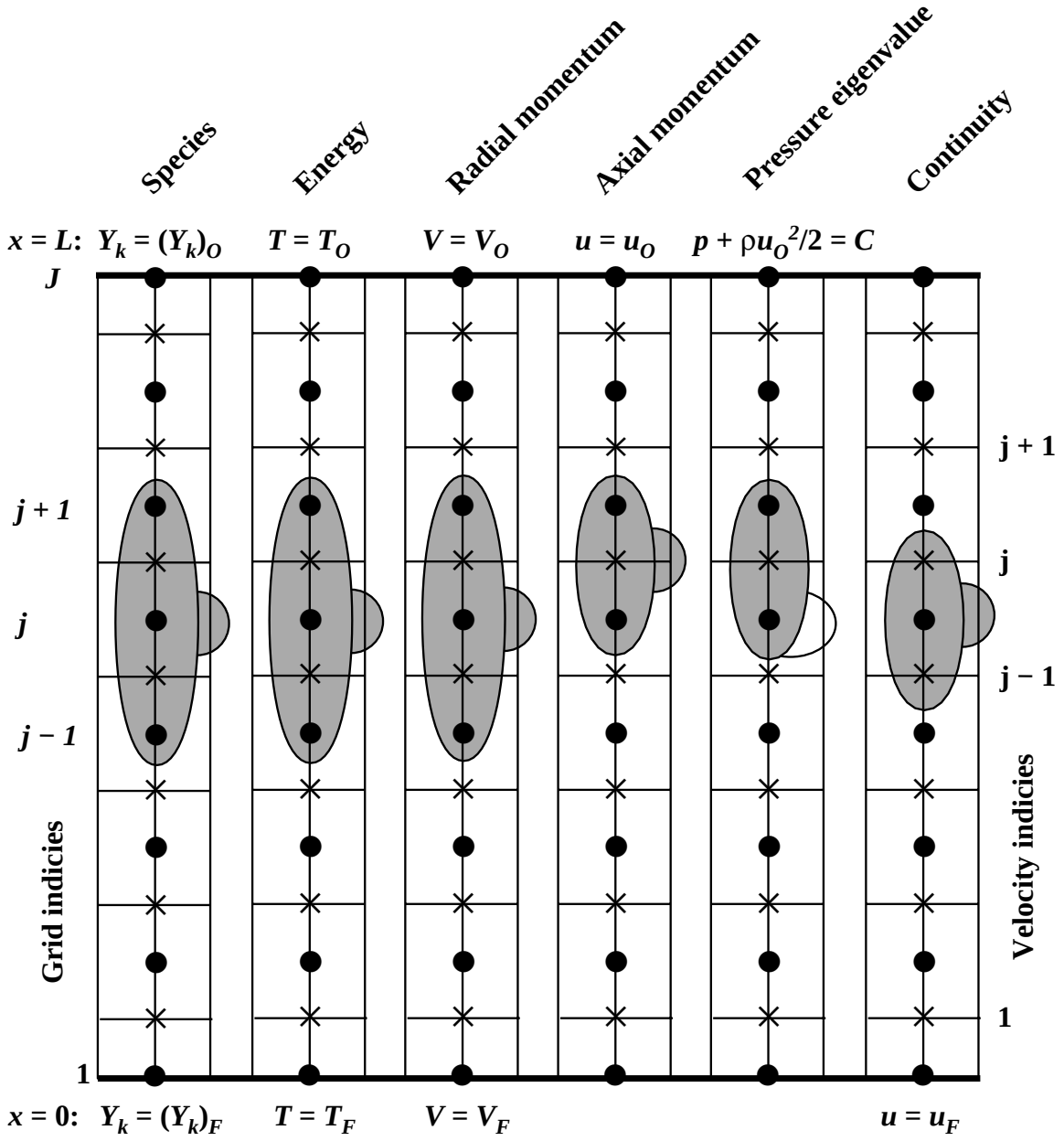

Figure 2: Schematic of the grid configuration using a finite-volume, staggered-grid spatial-difference stencil.

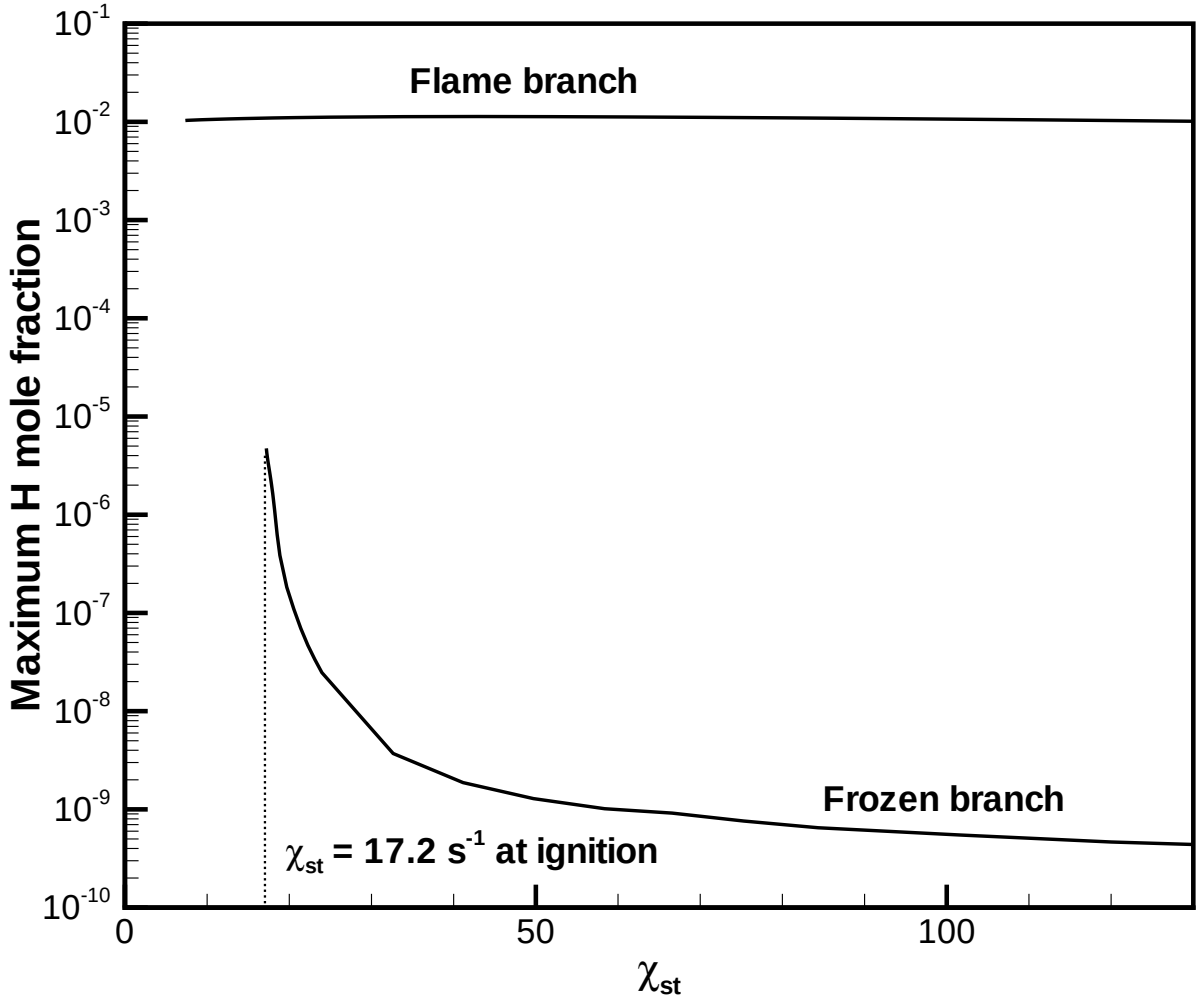

Figure 3: Maximum H mole fraction as a function of $\chi_{\rm st}$ for the steady ignition response.

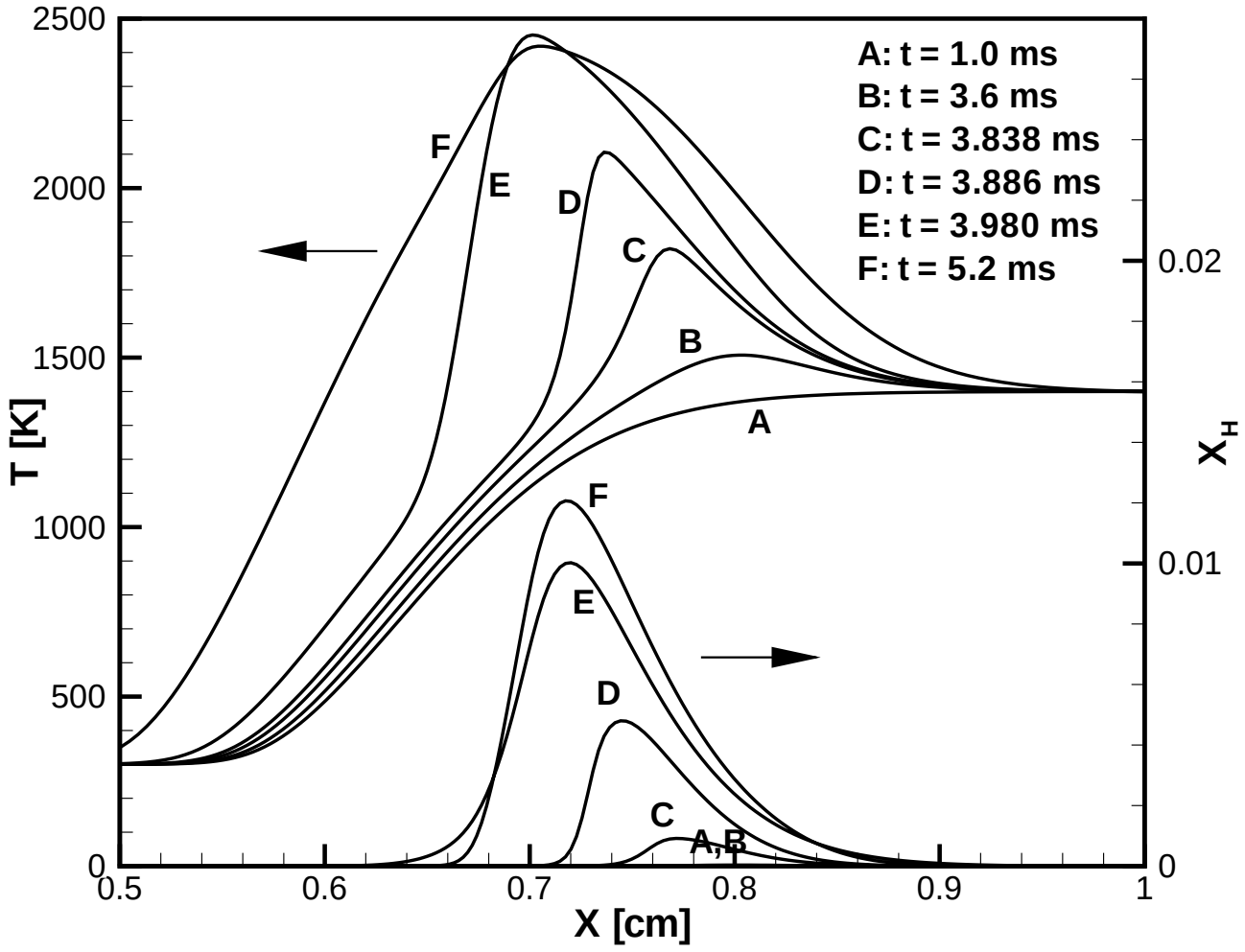

Figure 4: Evolution of temperature and H profiles during ignition for $u_0 = 1$ m/sec or $\chi_{\rm st} = 7.06$.

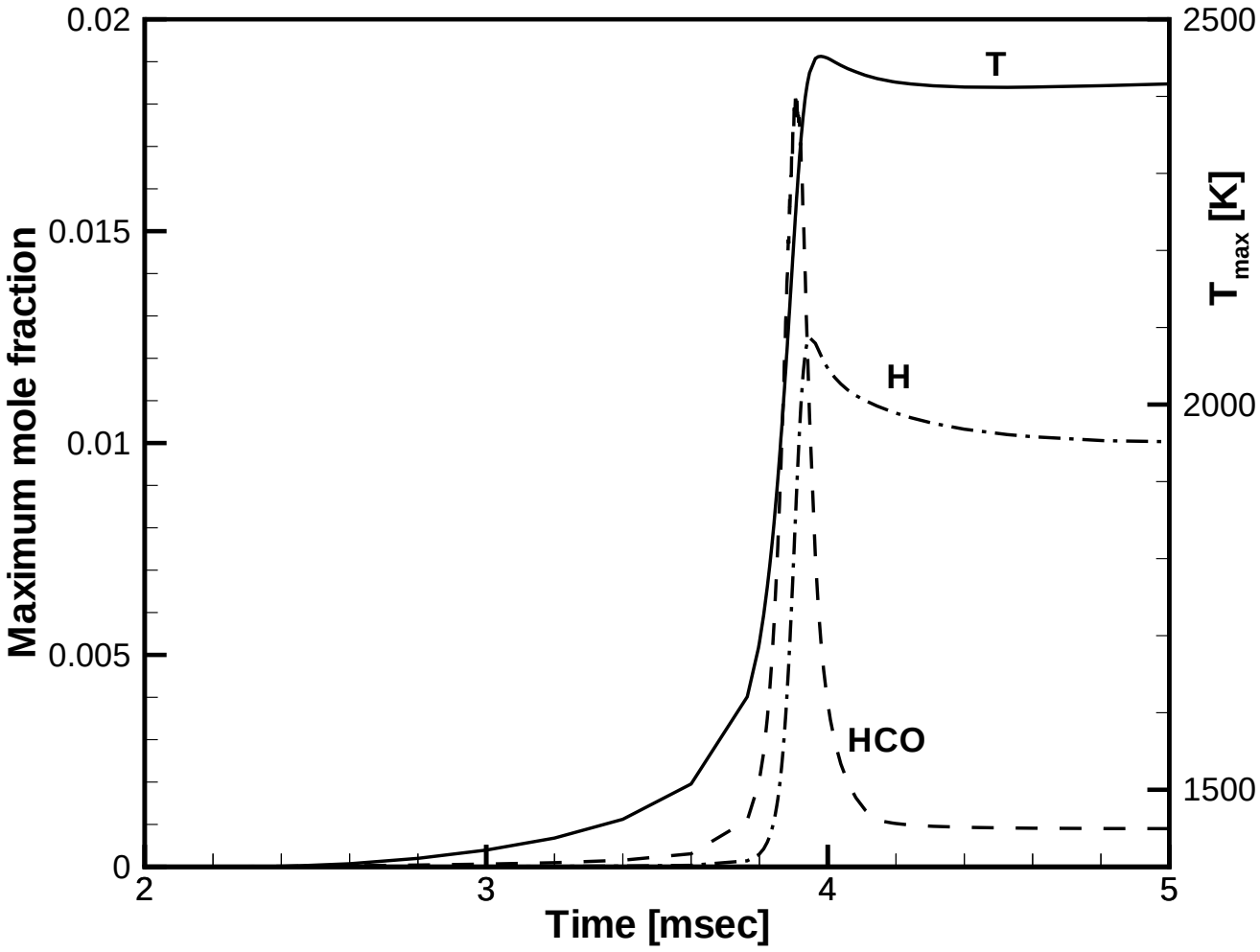

Figure 5: Transient evolution of the spatial maximum temperature, H and HCO mole fractions for $u_0 = 1$ m/sec or $\chi_{\rm st} = 7.06$.

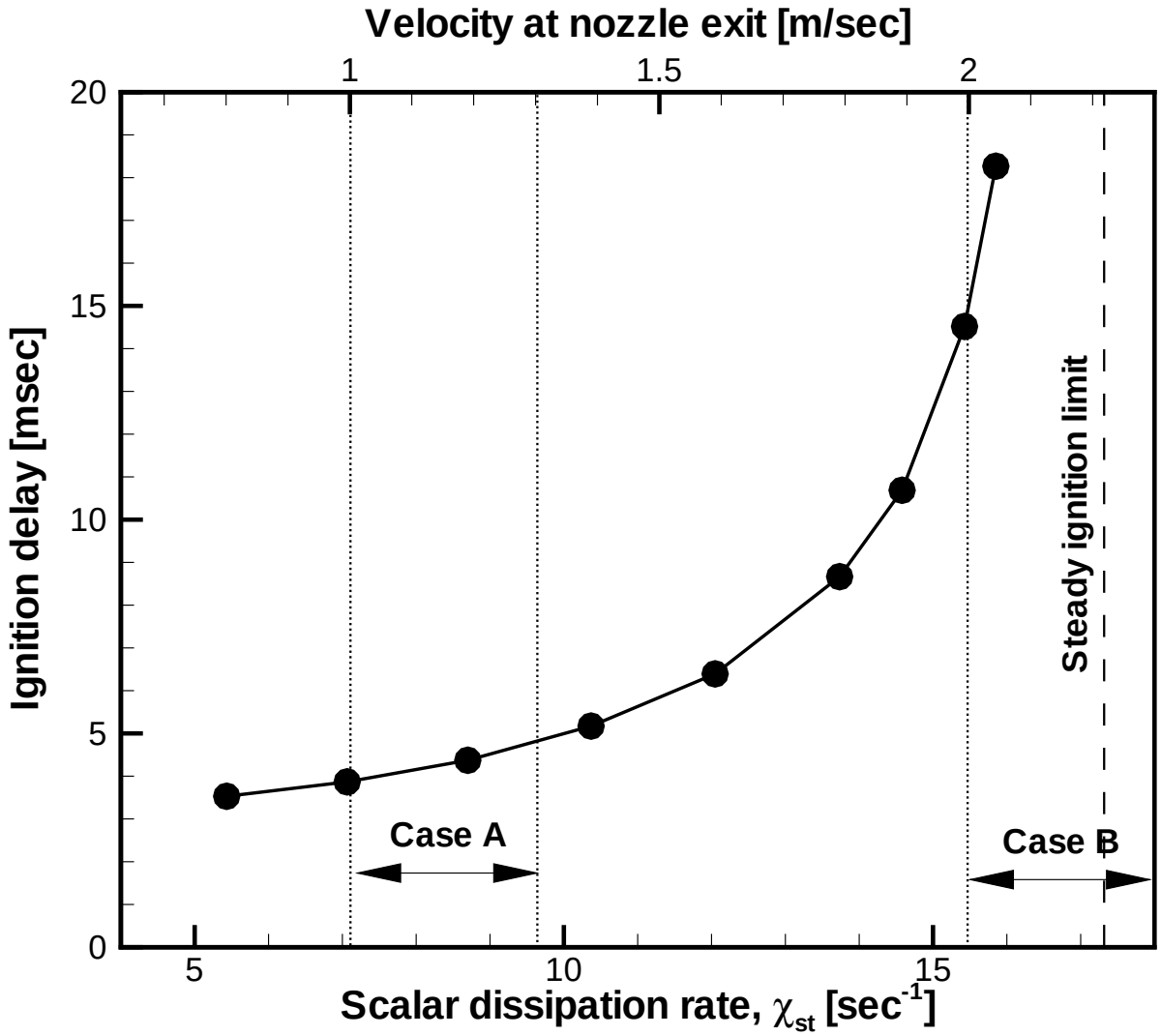

Figure 6: Ignition delay as a function of the scalar dissipation rate, demonstrating the sensitive response near the steady ignition limit. The arrows bounded by dotted lines denote the range of velocity oscillation used in the ignition under oscillatory strain rates.

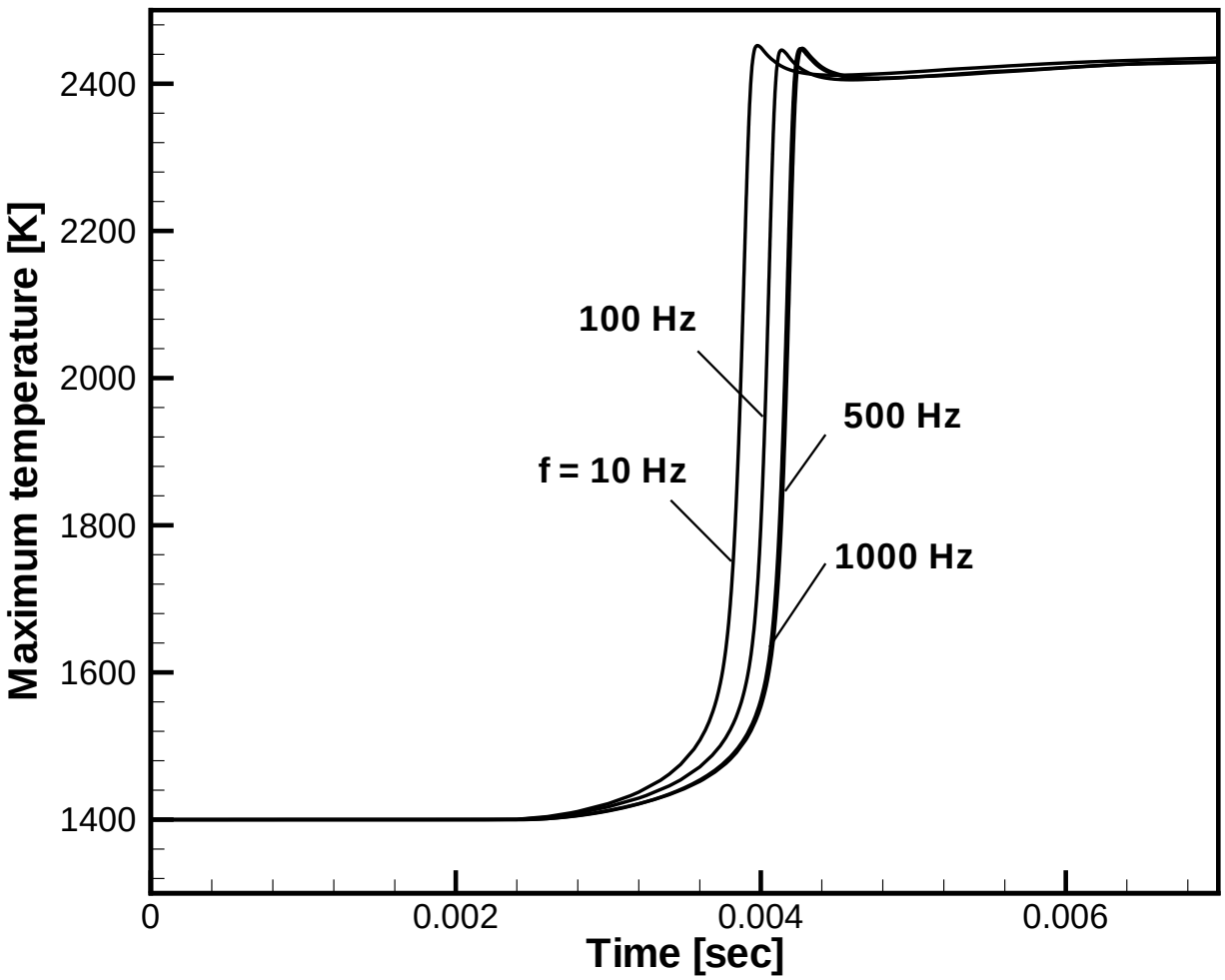

Figure 7: Temporal evolution of the maximum temperature under oscillatory strain rate for various frequencies; far from ignition limit, $u_0 = 1$ m/sec and $A = 0.15$.

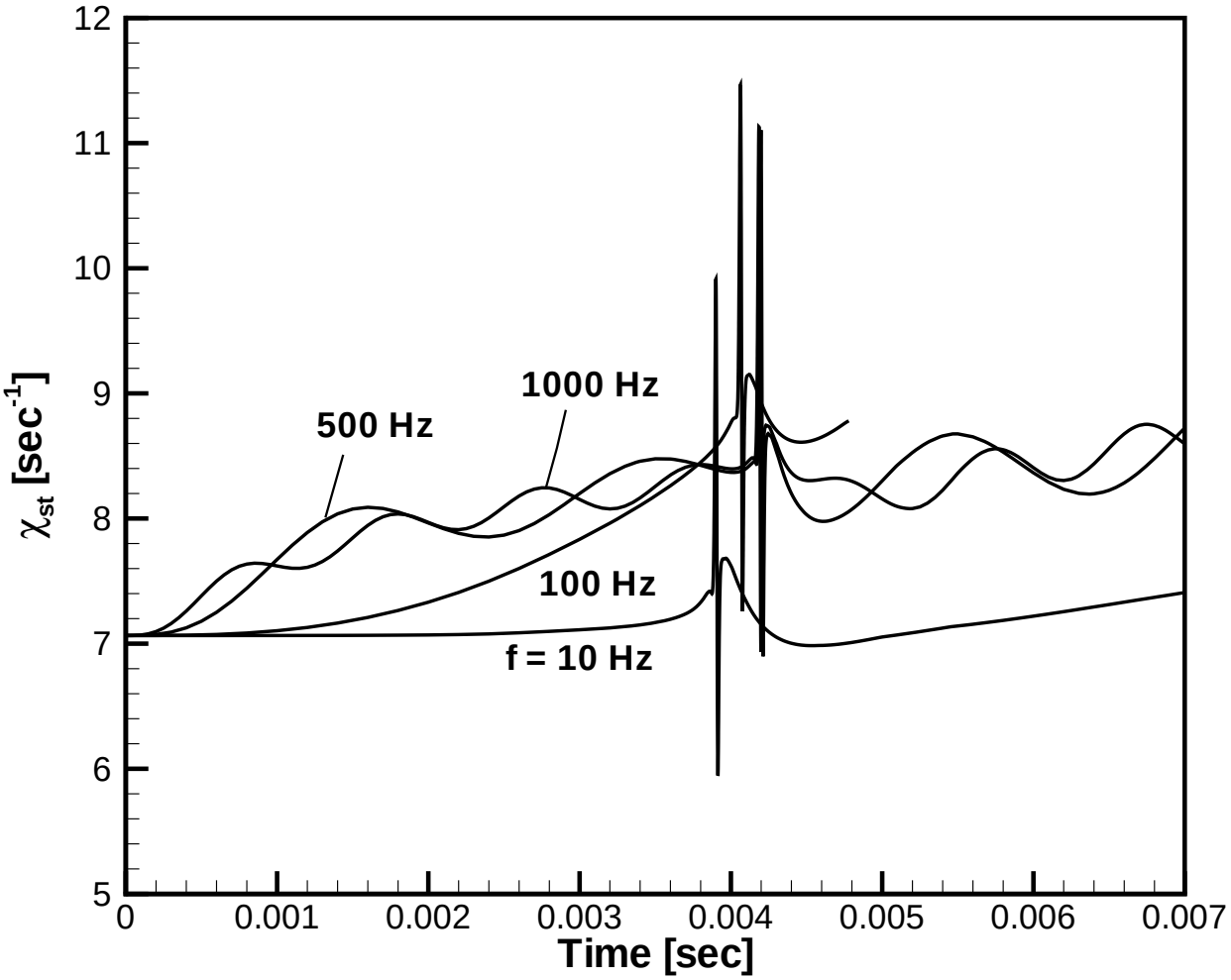

Figure 8: Temporal evolution of the scalar dissipation rate under oscillatory strain rate for various frequencies; far from ignition limit, $u_0 = 1$ m/sec and $A = 0.15$.

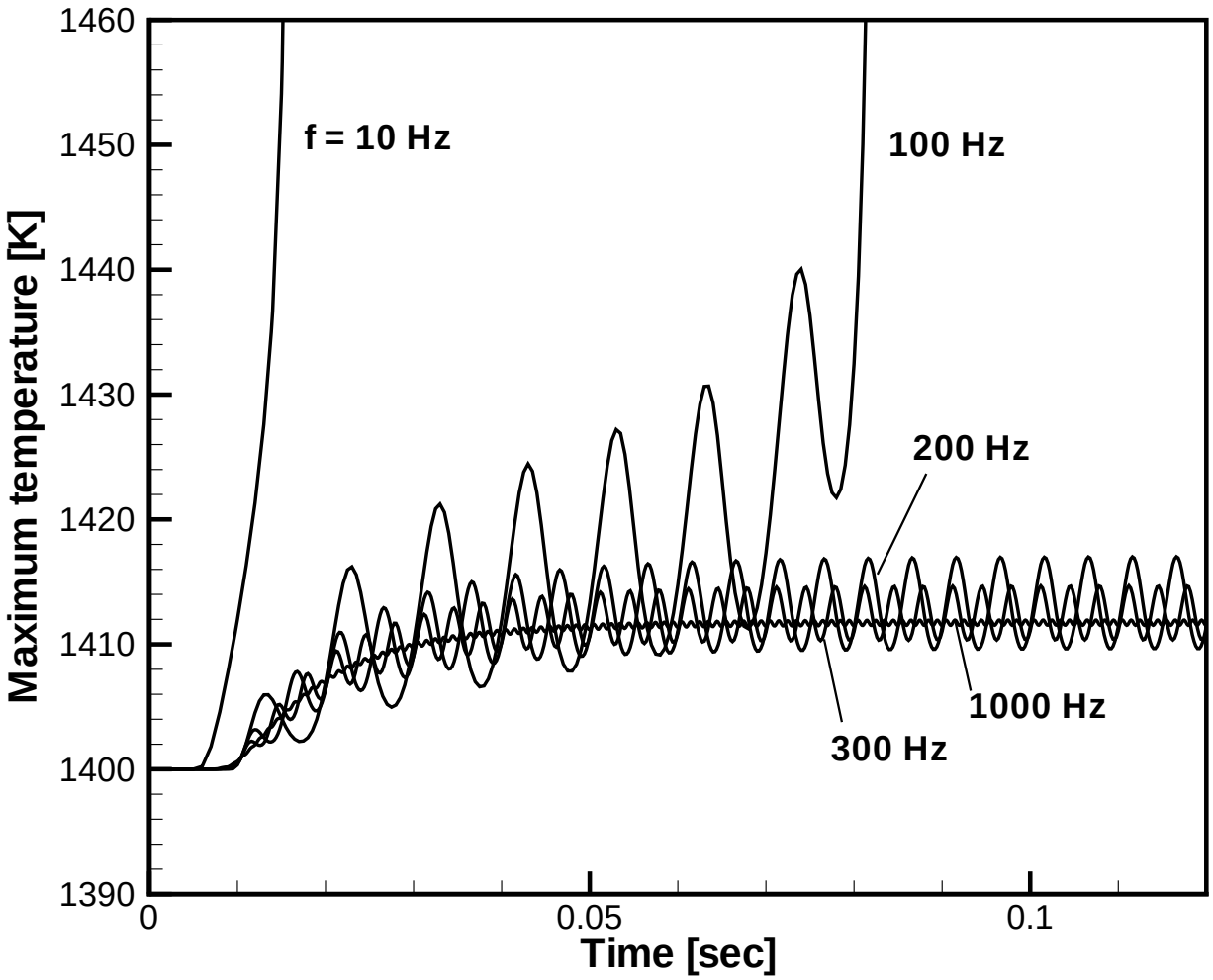

Figure 9: Temporal evolution of the maximum temperature under oscillatory strain rate for various frequencies; near ignition limit, $u_0 = 2$ m/sec and $A = 0.075$.

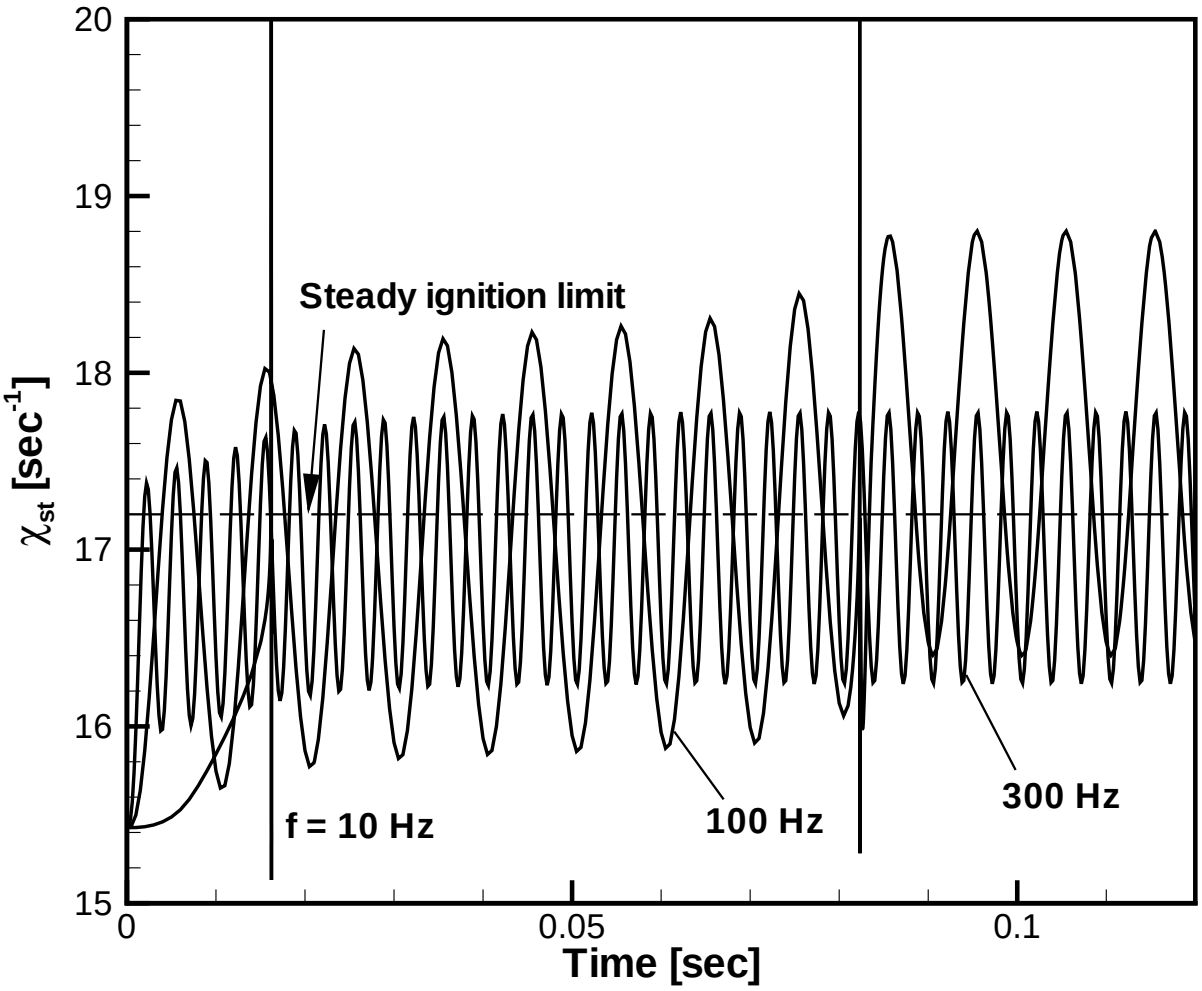

Figure 10: Temporal evolution of the scalar dissipation rate under oscillatory strain rate for various frequencies; near ignition limit, $u_0 = 2$ m/sec and $A = 0.075$. To avoid clutter, the $f = 200$ and 1000 cases are omitted.